Indian Journal of Chemistry
Vol. 55A, February 2016, pp. 177-181

Oxygen reduction reaction of manganese oxide/graphene oxide nanocomposite

K Pravinkumar[a], S Balaji[b,] *, T Manichandran[b], M Anandakumar[b] & G Kumaraguruparan[a]

[a]Department of Mechanical Engineering, Thiagarajar College of Engineering, Madurai 625 015, Tamilnadu, India

[b]Materials Technology Lab, Thiagarajar Advanced Research Centre, Thiagarajar College of Engineering, Madurai 625 015, Tamilnadu, India

Email: sbalaji@tce.edu

Received 17 July 2015; revised and accepted 29 January 2016

MnO_2/graphene oxide composite coating has been prepared by electrochemical anodic deposition method. Optimization of current density and deposition efficiency is reported. The formation of α-MnO_2/graphene oxide nanocomposite is elucidated through X ray diffraction and infrared reflection measurements. Morphological studies reveal the increase in porosity and exfoliation of graphene oxide by MnO_2 particles. The extent of oxygen reduction reaction occurring at the surface of MnO_2/graphene oxide composite coating have been analyzed by cyclic voltammetry and electrochemical impedance spectroscopy in aqueous 1 *M* Li_2SO_4 solution. The composite coating is observed to possess better catalytic properties towards oxygen reduction.

Keywords: Nanocomposites, Oxides, Graphene oxides, Oxygen reduction reaction, Manganese oxide

The energy storage devices have become indispensable components in most of the electronic equipments used for communication, remote sensing and automotive applications. Owing to the increasing functionality of electronic gadgets, the power demand by these equipment have also increased. However, the available footprint areas for energy storage devices are shrinking due to the miniaturization of electronic equipment. The key features expected from an energy storage device to be used in state of the art electronic equipment are (i) lightweight, thin with low footprint area demand, (ii) high cycle-life, float-life & low self-discharge, and, (iii) high power and energy density. Since lithium ion battery has most of the properties compatible with the need of electronic equipment, it is widely deployed as energy storage device[1]. Nevertheless, the power density and specific charge capacity of lithium ion battery is still inferior to the market demand. Hence concentrated efforts are being carried out by many research groups to explore new battery systems possessing gravimetric and volumetric energy, and power density higher than lithium ion batteries. In order to reduce the weight-to-volume ratio and in turn to increase the gravimetric energy density, metal-air batteries are being developed by many researchers[2,3]. One of the significant features of metal air batteries is oxygen reducing catalytic porous cathode material, which reduces the weight of the battery significantly and at the same time increases the specific capacitance of the cathode[4].

Though metal air battery technologies like zinc-air battery already exist, they are primary and non-rechargeable in nature[5]. This is mainly due to the irreversible nature of oxygen reduction reaction (ORR) and the corresponding irreversible product formation reaction in cathode and anode respectively. To address this issue, lithium air batteries are being developed, which have completely reversible byproduct[6] like Li_2O_2. In lithium air batteries, the anodes conventionally used for oxygen reduction are RuO_2, IrO_2 and Pt/C based composites and these anodes are basically noble metals and offer slow oxygen reduction kinetics[7]. Recently, researchers have started using graphene oxide based composites to increase the oxygen reduction reaction. To increase the electrocatalytic activity, graphene oxide MnO_2 has also been added[8]. MnO_2 is widely been preferred due to unassailable advantages like low cost, environment friendliness and high ORR kinetics[9]. However, the aggregation of graphene oxide in the presence of MnO_2 composite is perceived as a major issue. Moreover, the multistep complex preparation process of graphene oxide, MnO_2 and their composite is less attractive in the case of bulk production.

As an alternative to the existing methodologies to fabricate MnO_2/graphene oxide nanocomposite, the feasibility of their preparation by means of electrolytic co-deposition method has been demonstrated herein. The preparation of NiO attached graphene oxide nanocomposites by electrolytic co-deposition has already been investigated by Wu *et al.*[10] Graphene oxide are naturally negatively charged and hence are attracted by columbic forces of attraction towards the anode. Subsequent oxidation of Mn^{2+} to Mn^{4+} in the surface of graphene oxide takes place in the anode, resulting in MnO_2/graphene oxide nanocomposite[11]. The structural, morphological and electrochemical properties of the MnO_2/graphene oxide nanocomposites are also reported herein.

Experimental

MnO_2 film was prepared by the electrodeposition method from the electrolyte containing 0.5 *M* manganese acetate tetrahydrate (Merck) and 0.5 *M* sodium sulfate (Merck). The deposition was carried over 0.3 mm AS316 stainless steel (SS) substrate. Prior to the deposition, the substrate was degreased in acetone followed by ultrasonic cleaning in doubly distilled water for 30 min. To optimize the current density for electrodeposition, Hull cell experiments were carried out by applying 30 mA for 10 min. As a result of the current density variations in the substrate, the quality of the deposit varied with respect to length of the electrode. The adherent, less porous deposit was observed in the anode area corresponding to the current density 0.6 mA/cm^2 and hence this current density was identified as optimized current density. Further experiments were carried out in this current density for 30 min on SS electrode. The oxidation reaction occurring at SS electrode (anode) is as follows:

$$Mn^{2+}\ (electrolyte) \rightarrow Mn^{4+} + 2e^- \quad \ldots(1)$$

$$Mn^{4+} + 2\ e^- + O_2 \rightarrow MnO_2\ (deposited\ at\ SS\ electrode) \quad \ldots(2)$$

Graphene oxide (GO) was synthesized by modified Hummers method from a precursor containing 15 g of $KMnO_4$ (Sigma Aldrich), 5 g of graphite powder (Sigma Aldrich) dissolved in 115 mL of H_2SO_4 (98%) (Merck)[12] . The precursor was prepared under controlled temperature ~10 °C and the *p*H was maintained at ~5. Then the precursor was subjected to continuous stirring at 90 °C for 5 h and filtered and dried under vacuum for 110 °C for 1 h. Fine GO powder was used to prepare the MnO_2/GO composite through electrodeposition method.

The MnO_2/GO electrodeposition bath was prepared by adding 1.5 g L^{-1} of synthesized GO powder in the MnO_2 plating bath. The electrodeposition of MnO_2/GO was carried out with current density of 0.6 mA/cm^2 for 30 min in SS substrate. For the homogenous MnO_2/GO composite preparation, the plating was carried out under mechanical stirring at 600 rpm and ultrasonication. The structural properties of MnO_2 and MnO_2/GO films were characterized by XRD using Philips PW 1710 X ray diffractometer and the structural parameters were studied by Powder X software. Morphological analysis of the films was carried out by scanning electron microscopy (Tescan SBH). The morphological parameters like surface roughness, porosity, pore area were calculated using the Image J software[13]. The morphology of the coatings were further elucidated by atomic force microscopy. The oxygen reduction reaction of the samples and their electrochemical impedance were recorded using Micro Autolab electrochemical workstation in 1.0 *M* Li_2SO_4 electrolyte. The MnO_2 and MnO_2/GO films were used as working electrode, while platinum and saturated calomel electrodes were used as counter and reference electrodes respectively.

Results and discussion

The structural properties of the materials are analyzed using X-ray diffraction and infrared spectroscopy. The XRD patterns of MnO_2/graphene nanocomposite prepared under mechanical stirring and ultrasonication show the presence of α-MnO_2 peaks that are formed while electrodeposition (Fig. 1(a & b)), as per JCPDS reference file 530633. Song *et al.*[14] have reported that among the various to undergo fast electrochemical reaction without

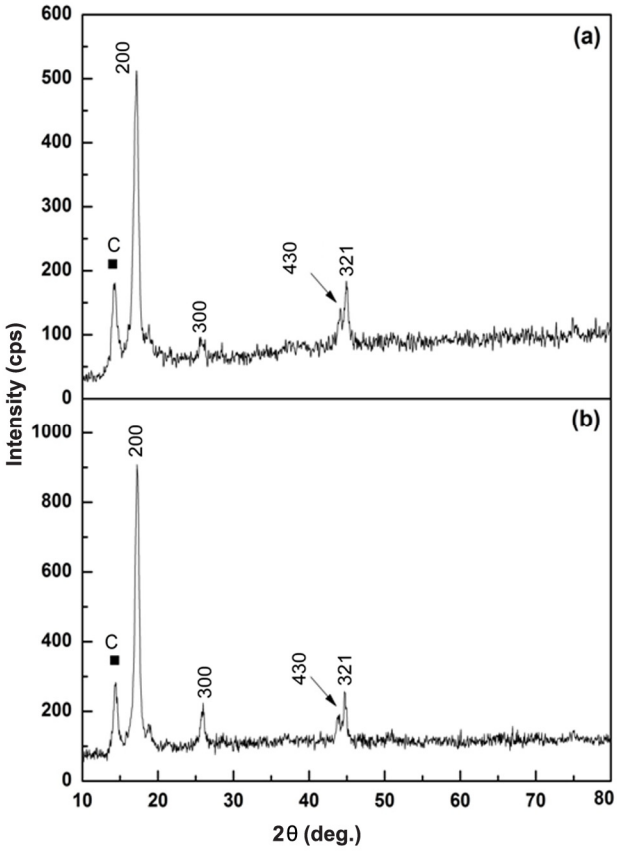

Fig. 1 – X-ray diffraction patterns of MnO_2/graphene nanocomposite prepared by (a) ultrasonication, and, (b) mechanical stirring.

polymorphic forms of MnO_2, α-MnO_2 has the ability structural distortion. Hence, electrochemical method is a facile way to synthesize α-MnO_2 coatings. In order to increase the conductivity of α-MnO_2 coatings, graphene oxide has been co-deposited along with MnO_2. The XRD patterns of MnO_2/graphene oxide composite powders synthesized by stirring and ultrasonication are identical except for the peak intensity. The peak intensity is observed to decrease on ultrasonication and this may be attributed to the reduction in crystallite size during ultrasonication. The structural parameters derived from XRD measurements are presented in Table 1. The α-MnO_2 formed while stirring has undergone lattice elongation in *c* axis. However, the α-MnO_2 formed while ultrasonication has not suffered from any such distortion. Hence, it may be assumed that electrodeposition with ultrasonication is best suited for preparation of α-MnO_2 coatings. The graphene oxide powders dispersed in the electrolyte show a peak at around 14.27° as seen in Fig. 1a and 1b; according to the JCPDS reference file no. 500926, it may be attributed to hexagonal type carbon.

FTIR spectrum of graphene oxide shows vibrational bands at around 3425, 1714, 1600, 1100 and 468 cm^{-1} corresponding to –OH group, C=O stretching, C-C stretching, C-O stretching, C-O bending respectively. The vibrational and around 1600 cm^{-1} is due to stretching of sp^2 C-C bond present in graphene oxide[15]. This may be assumed as a fingerprint for the unaltered hexagonal arrangement of carbon in graphene oxide. Moreover, the presence of peaks around 1714 cm^{-1} and 1100 cm^{-1} corresponding to C=O and C-O stretching shows the successful cleavage of graphite lamellar layer and subsequent oxidation of armchair carbon and the peripheral carbon[16].

The FTIR spectrum of MnO_2/graphene oxide composite prepared by ultrasonication shows blue shift in the vibrational bands corresponding to –OH group, C=O and C-C stretching. This may be attributed to the stiffening of C-C bond in graphene oxide due to the presence of Mn-O_6 octahedral arrangement around graphene oxide and also due to the presence of defects in graphene oxide[17]. This may be attributed to the hydrophilic nature of graphene oxide resulting in higher dispersion with Mn^{2+} ions in the electrolyte. The Mn^{2+} ions have the possibility to interact with every single atom of graphene oxide and form a lamellar composite structure with graphene oxide. During oxidation of Mn^{2+} ions, the graphene oxide acts as buffer for shuttling of electrons over some distance in the electrolyte and hence acts as a nucleation point for MnO_2 formation. The spectrum also shows that the intensity of vibration corresponding to –OH group has increased during formation of the composite. This may be attributed to the -COOH formation at the end of the graphene oxide chain[18]. A new peak around 2350 cm^{-1} corresponding to carboxylic group stretching substantiates the above assumption.

Figure 2 shows the morphological features of electrodeposited MnO_2 and MnO_2/GO materials using scanning electron microscopy. The micrograph of MnO_2 shows the pristine crystalline MnO_2 grains formed during electrodeposition and this is in good

Table 1 – Structural and morphological parameters and impedance data of MnO_2/graphene oxide

Parameter	MnO_2/graphene oxide	
	Stirring	Ultrasonication
Crystallite size (nm) (± 0.1)	11.8	9.5
Lattice strain (±0.001)	0.0029	0.0036
Porosity (%) (±0.1)	31.4	38.5
Aspect ratio	1.354	1.291
Surface roughness(nm)		
R_a	135	132
R_q	132	141
$R_{CT\ (ohm)}$	31.38	38.46
$C_{dl\ (uF)}$	1.354	1.291

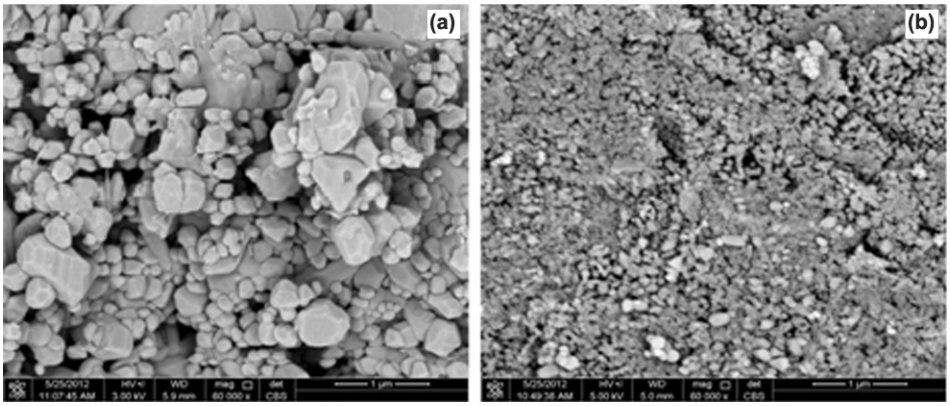

Fig. 2 – Scanning electron micrographs of (a) MnO_2, and, (b) MnO_2/graphene oxide nanocomposite.

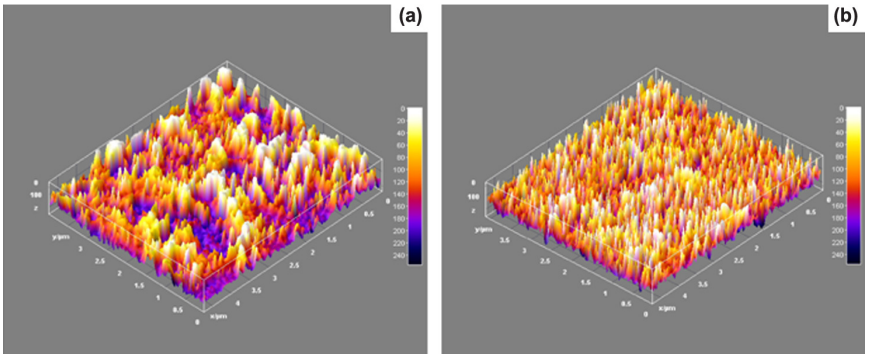

Fig. 3 – Atomic force micrograph of (a) MnO_2, and, (b) MnO_2/graphene oxide nanocomposite.

concomitance with the observations from XRD studies. On inclusion of graphene oxide with MnO_2, significant reduction in grain sizes is observed. Hence, it may be inferred that the graphene oxide prevents the agglomeration of MnO_2 into coarse aggregates. The porosity of MnO_2 is observed to increase with graphene addition. However, the surface roughness values calculated from AFM image remains unchanged (Fig. 3). The morphological parameters derived from SEM and AFM are presented in Table 1.

The MnO_2 and MnO_2/GO samples were tested for oxygen reduction capacity by cyclic voltammetry in the potential range –0.4 to 1.4 V at a scan rate of 5 mV/s. The cyclic voltammograms of the MnO_2 and MnO_2/GO electrodes in 1 *M* Li_2SO_4 electrolyte are presented in Fig. 4a. The area covered between oxidation and reduction pathways are observed to increase due to the presence of graphene oxide in MnO_2; this may be attributed to the increase in electrochemical active surface area[13]. The MnO_2 electrode exhibits reduction peak around 0.9 V, attributed to the reduction of dissolved oxygen present in the electrolyte. The plausible reduction reaction is as follows (Eqs 3-5).

$$Mn^{4+} + e^- \rightarrow Mn^{3+} \quad \text{(fast)} \quad \ldots(3)$$

$$Mn^{3+} + O_2 \rightarrow Mn^{3+}\text{-}O_2, \text{ ads} \quad \text{(fast)} \quad \ldots(4)$$

$$Mn^{3+} \text{–O2, ads} \rightarrow Mn^{4+} \text{–} O^{2-}\text{,ads} \quad \text{(slow)} \quad \ldots(5)$$

Initially, the Mn^{4+} in the electrode reduces to Mn^{3+} according to Eq. (3) and becomes active site for the adsorption of O_2 (ads) according to Eq. (4). The adsorbed oxygen act as electron acceptor due to its high electronegativity and accepts one electron from Mn^{3+} and results in Mn^{4+}-O^{2-} product (Eq. 5). In the presence of graphene oxide, the reduction peak

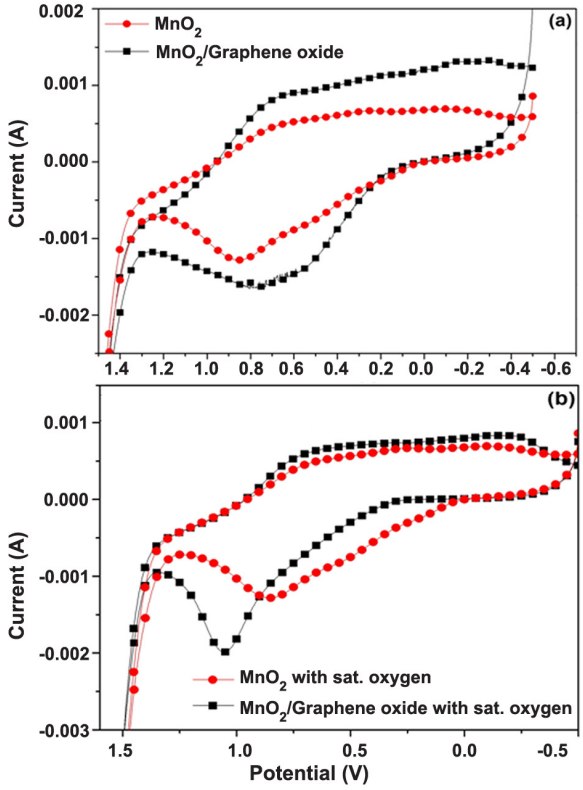

Fig. 4 – CVs of MnO_2 and MnO_2/GO electrodes. [(a) in 1 *M* Li_2SO_4; (b) in oxygen saturated 1 *M* Li_2SO_4].

broadens and this may be due to the exfoliation of graphene oxide by the MnO_2. As a result the electrolyte has more active sites available for reduction[15]. Similarly, in the oxidation pathway, release of electron and subsequent evolution of oxygen is observed near 0.7 V for MnO_2 and MnO_2/GO electrodes. The CV of the electrodes in the oxygen saturated 1 *M* Li_2SO_4 electrolyte presented in Fig. 4b shows that the half-wave onset potential for oxygen reduction is shifted towards positive value for MnO_2/graphene oxide electrode, indicating the higher oxygen reduction activity of MnO_2/graphene oxide electrode[19].

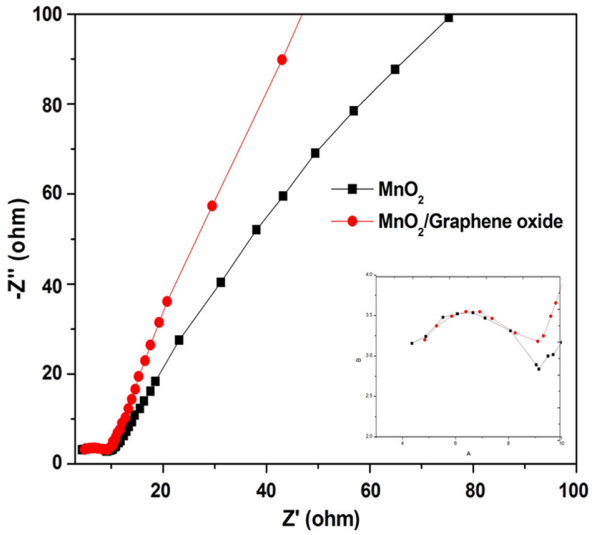

Fig. 5 – Impedance spectra of MnO_2 and MnO_2/graphene oxide composite.

The AC impedance characteristics of the MnO_2 and MnO_2/GO electrodes were tested in the frequencies ranging from 1 mHz to 1 MHz and the resultant Nyquist plots are presented in Fig. 5. Both the electrodes show the presence of semicircle in high frequencies followed by straight line in low frequencies. The high frequency semicircle may be attributed to the single electron transfer occurring in the process shown in Eqs (3), (4) and (5). The numerical value of the diameter of the semicircle is approximately equal to the charge transfer resistance offered by the electrode. From the Fig. 5, it is evident that while introducing graphene oxide into MnO_2, the charge transfer resistance decreases and this effect highlights the contribution of graphene oxide in improving the conductivity of pristine MnO_2 electrode. The reduced charge transfer resistance due to graphene oxide is responsible for the improvement in oxygen reducing catalytic effect of MnO_2/GO composite. Moreover, from Fig. 5 it may also be observed that the presence of graphene oxide does not increase the double layer capacitance of the MnO_2 electrode. The parameters calculated from impedance analysis are presented in Table 1. The Warburg diffusion plots of the electrodes were linear for both the electrodes, illustrating more diffusion in the case of MnO_2/GO electrode. This effect may be attributed to the exfoliation of graphene oxide layer by MnO_2, facilitating more ions to diffuse in the free space between graphene oxide.

The present study demonstrates that co-deposition of MnO_2/GO composite is a facile way to synthesize composite functional coatings. From XRD patterns, it is inferred that the simultaneous ultrasonication of graphene oxide during electrodeposition of MnO_2 is efficient in preparation of MnO_2/GO composite coating. IR analysis shows the defect in graphene oxide due to its exfoliation by MnO_2 particles. This exfoliation results in higher porosity for MnO_2/GO composite as elucidated from SEM results. From the electrochemical measurements, it is inferred that the MnO_2/GO composite coating has low over-potential for oxygen reduction as compared to MnO_2. It may be concluded that in terms of structural stability, morphology and electrochemical activity, the MnO_2/GO electrodes are far superior than pristine MnO_2 electrodes.

Acknowledgement

The authors thank Department of Science and Technology, New Delhi, India, for financial support to carry out the work under Young Scientist scheme.

References

1 LaO G J, In H J, Crumlin E, Barbastathis G & Horn Y S, *J Energy Res,* 31 (2007) 548.
2 Armand M & Tarascon J M, *Nature,* 451 (2008) 652.
3 Rahman M A, Wang X & Wen C, *J Appl Electrochem,* 44 (2014) 5.
4 Hardwick L J & Bruce P G, *Curr Opin Solid State Mater Sci,* 16 (2012) 178.
5 Yanguang L & Dai H, *Chem Soc Rev*, 43 (2014) 5257.
6 Ogasawara T, Débart A, Holzapfel M, Novák P & Bruce P G, *J Am Chem Soc,* 128 (2006) 1390.
7 Cheng H & Scott K, *Appl Catal,* B108 (2011) 140.
8 Park H W, Lee D U, Liu Y, Wu J, Nazar L F & Chen Z, *J Electrochem Soc,*160 (2013) 2244.
9 Yang Y, Shi M, Li Y-S & Fu Z-W, *J Electrochem Soc,* 159 (2012) 1917.
10 Wu M-S, Lin Y-P, Lin C-H & Lee J-T, *J Mate*r Chem, 22 (2012) 2442.
11 Chen J, Yao B, Li C & Shi G, Carbo*n*, 64 (2013) 225.
12 Song J, Wang X & Chang C-T, *J Nanomater*, 2014 (2014) doi.org/10.1155/2014/276143.
13 Balaji S R K, Mutharasu D, Shanmugan S, Sankara Subramanian N & Ramanathan K, *Ionics*, 16 (2010) 351.
14 Song Z, Liu W, Zhao M, Zhang Y, Liu G, Yu C & Qiu J, *J Alloys Comp*, 560 (2013) 151.
15 Cheng Q, Tang J, Ma J, Zhang H, Shinya N & Qin L-C, *Carbon,* 49 (2011) 2917.
16 Zhang Y, Su M, Ge L, Ge S, Yu J & Song X, *Carbon,* 57 (2013) 22.
17 Li Z, Zhang P, Wang K, Xu Z, Wei J, Fan L, Wu D & Zhu H, *J Mater Chem,* 21 (2011) 1324.
18 Krishnamoorthy K, Navaneethaiyer U, Mohan R, Lee Je & Kim S-J, *Appl Nanosci,* 2 (2012) 119.
19 Prabu M, Ramanakrishnan P & Shanmugam S, *Electrochem Commun*, 41 (2014) 59.